

Mesh Deformation Based Finite Element - Fictitious Boundary Method (FEM-FBM) for the Simulation of Twin-screw Extruders

O. Mierka, T. Theis, T. Herken, S. Turek, V. Schöppner, F. Platte

November 24, 2014

Abstract

In this paper a novel computational strategy consisting of a special combination of numerical techniques is presented, which allows to perform flow simulations in the framework of co-rotating twin-screw extruders involving complex geometrical descriptions of rotating intermeshing internal boundaries. The individual techniques combined together are a *a)* higher order Finite Element Method (FEM) augmented with the *b)* Fictitious Boundary Method (FBM) and a novel *c)* PDE-free Mesh Deformation (MD) technique, guaranteeing a high resolution/high order numerical scheme without the necessity of a case-specific time-consuming preprocessing step foregoing each simulation. The designed numerical scheme has the clear advantage to be used in a fully automated environment suitable to perform detailed case studies playing a key role in the design of specific twin-screw machines for particular material processing applications.

keywords: extruder simulation, CFD, Fictitious Boundary Method, Mesh Deformation, FEM

1 Introduction

Material substitution, which is taking place due to the numerous advantages offered by plastics has led to an above average growth rate of polymer processing and manufacturing in the last few years. The driving force of this phenomenon is mainly related to the replacement of traditional materials such as metal, glass and paper with relatively cheaper and lighter plastics. Furthermore, the properties determined by the requirements put on the products can be fine-tuned by additional compounding processes, which is an other considerable benefit. Co-rotating twin-screw extruders (CRTSE) are currently used in compounding processes due to their modular structure, and due to their ability to provide intensive mixing associated to relatively short residence times. In order to optimize the compounding process and to further improve the quality of the products, the exact understanding of the underlying processes is essential. From the point of view of experimental observations, especially in light of the high complexity of the interdependent operations, one has to cope with time-consuming experimental investigations. To this end, in future (if not already now) simulations may offer themselves as an alternative way of investigation assuming that their feasibility - following current trends in computer science

and computational fluid dynamics (CFD) - will further improve. The most promising role of CFD lies in the prediction capabilities of safe (w.r.t the processed material) and efficient operation of twin-screw extruders (TSE), which can be achieved via simultaneous simulations of different setups associated with different screw geometries and gap sizes, being mostly responsible for the pressure built-up and extent of friction resulting in corresponding temperature increase. Furthermore, simulation results can be postprocessed in many different ways so to recover important quantities, like pressure drops, axial temperature profiles, specific energy input, residence time distribution or fractional distribution of shear rates, which otherwise in terms of experimental observation can not be simultaneously (if at all) measured. Originally, the process and flow simulation of a CRTSE was based on one-dimensional models [15], which were in charge to predict important process parameters (such as temperature or pressure build up along the axial length of the screw) without considerable computational time. On the other hand, essential problems of these simplified computational models are related to the assumption of homogeneous cross-sectional distributions of quantities, which directly exclude the possibility of prediction of anisotropic shear rate distributions, and therefore are unable to quantify the appearance of hot-spots which may have a dramatic influence on the inhomogeneously processed material (i.e. initiation of unwanted vulcanization while processing natural/synthetic rubber). As an improvement, two-dimensional models are used to take into account of the gradients. These (still) simplified models have an important advantage compared to the three-dimensional simulations due to the significantly lower computational requirements. Currently used industrial one- or two-dimensional simulation programs of CRTSE are Akro-Co-Twin-Screw (University of Akron), Ludovic (CEMEF, France), TXS (Polytech, USA) and SIGMA developed at the University of Paderborn. As a result of recent development, the simulation program SIGMA presents the option to perform additional fully three dimensional studies based on the corresponding CFD extension Extrud3D, which covers the simulation of fully-filled TSE segments consisting of conveying/kneading elements as well as their mutual combinations. The newly developed Extrud3D module is an extension of the open source Finite Element (FEM) based CFD package FEATFLOW [13, 14], which was originally developed by S. Turek and his group at TU Dortmund and has proven to exhibit outstanding numerical properties while taking part in various CFD benchmark initiatives [2, 5, 6, 10] covering a wide range of applications. Thanks to the incorporated Fictitious Boundary Method (FBM) [10] the resulting fully-automated parallel 3D simulation tool enables the simulation of fully-filled CRTSEs without relying on in-depth expertise in CFD of the user, since all kinds of preprocessing operations (mainly related to mesh generation) are intrinsically embedded into the simulation tool. From the available software packages used for full-three dimensional simulations (up to the knowledge of the authors) are ANSYS-PolyFlow, an XFEM-based code development from the group of Anderson (Eindhoven University of Technology) [11, 12], OpenFOAM (commercial release of Wikki Ltd.) and a specific in-house code of Bayer Technology Services [9], which on the one hand are successfully used for industrial purposes, but on the other hand partially suffer from the shortcomings stemming from:

- cumbersome geometrical preprocessing - in terms of meshing
- simplified models - neglecting the non-Newtonian rheological effects
- total computational performance - computational performance vs. accuracy

Besides the discretization and the individual shortcomings, the main difference between the CFD tools mentioned above lies in the treatment of internal moving boundaries. Their treatment can be in practise performed on the basis of a remeshing (A) [11, 12], mesh deformation (B) or fictitious boundary method (C). Without doubts, each of these techniques has its pros and cons, which depending on the given application may prevail in favour of one against the others. Clear advantages of (A) and (B) are related to the arising aligned computational meshes, which on the other hand, especially in case of complex time-dependent geometries (i.e. CRTSEs) may become inefficient, if not impossible (i.e. in case of a hexahedral meshes). Improvements of (A) in the framework of TSE simulations have been presented on the basis of

- sliding meshes, so that the two individual barrels of the TSE are meshed independently, and the coupling between them is performed in terms of interpolation (used by OpenFOAM-Wikki Ltd, and ANSYS-PolyFlow). There are, however, two main disadvantages related to this approach: 1) a computational one according to which a dominant "block-Jacobi" effect is introduced into the solution of the linear systems influencing negatively the global convergence behavior of the computations, 2) a practical one which excludes realistic twin-screw simulations of intermeshing screws (i.e. the screw barrels are overlapping each other).
- local adaptivity (XFEM based simulation tools), which on the one hand guarantees a high resolution of the boundaries (especially in the gap regions), on the other hand introduces difficulties in terms of load balancing in a parallel solver framework and inhibits the use of highly efficient multigrid techniques due to the arising complexity of the generated fine structured elements.

From the point of view of TSE simulations (presence of dramatic topological changes of the computational domain), the technique (B) is unusable, *unless* only partial alignment of the mesh is requested, which implies the additional use of technique (C). Summarising the advantages of the technique (C) one should mainly emphasize the constant matrix structures, relatively easy meshing, since the computational mesh does not need to be aligned. This property in addition guarantees the existence of a relatively coarse mesh being appropriate for multigrid-based solvers, which exhibit superior performance properties during the solution of the arising linear systems even in a parallel (on the basis of domain decomposition) framework. As it has been indirectly already mentioned, the ultimate technique offers itself as the combination of techniques (B) and (C) which will be presented in this article and is demonstrated on the chosen numerical examples.

2 Governing equations, discretization and mathematical modeling

As usual [8, 11, 16], we neglect the inertial terms due to the dominant viscous forces, and therefore the flow of molten polymers is described by the unsteady incompressible Stokes equations, as follows:

$$\begin{cases} \rho \partial_t \vec{v} + \nabla p = \nabla \cdot \mathbb{S} \\ \nabla \cdot \vec{v} = 0 \end{cases} \quad (1)$$

Here, \mathbb{S} is the viscous stress tensor $\mathbb{S} = \eta(\nabla\vec{v} + \nabla\vec{v}^T)$, ϱ is the constant density, η represents the shear-dependent viscosity, and the pair (\vec{v}, p) are the unknown velocity and pressure.

The discretization of the governing equations is performed on the basis of the Finite Element Method (FEM), and in particular the corresponding extensions are implemented into the open-source CFD package FEATFLOW. For the time discretization the basic one-step Θ -scheme is used, which allows in general the selection of the fully implicit Crank-Nicolson ($\Theta = 0.5$) or Backward Euler-Scheme ($\Theta = 1$). Corresponding to the individual temporal discretization scheme the following system is obtained:

For given \vec{v}^{n-1}, p^{n-1} and $\Delta t = t_n - t_{n-1}$, solve the following system

$$\begin{cases} \varrho(\vec{v}^n - \vec{v}^{n-1}) + \Delta t\Theta(\nabla \cdot (\eta(\nabla\vec{v}^n + (\nabla\vec{v}^n)^T))) + \Delta t\nabla p^n = \\ \quad = \Delta t(\Theta - 1)(\nabla \cdot (\eta(\nabla\vec{v}^{n-1} + (\nabla\vec{v}^{n-1})^T))) \\ \nabla \cdot \vec{v}^n = 0, \end{cases} \quad (2)$$

which is then discretized further in space in the framework of FEM on the basis of a high order Q_2/P_1 pair of elements [2, 10]. According to Galerkin FEM, the Stokes equations are formulated as a variational problem, which in this particular case results in the following system of equations:

$$\begin{cases} M_{\varrho l}\hat{u}_h^n + \Delta t\Theta\left(S^{11}\hat{u}_h^n + S^{12}\hat{v}_h^n + S^{13}\hat{w}_h^n\right) - \Delta tB^1\hat{p}_h^n = (rhs^n)_1 \\ M_{\varrho l}\hat{v}_h^n + \Delta t\Theta\left(S^{21}\hat{u}_h^n + S^{22}\hat{v}_h^n + S^{23}\hat{w}_h^n\right) - \Delta tB^2\hat{p}_h^n = (rhs^n)_2 \\ M_{\varrho l}\hat{w}_h^n + \Delta t\Theta\left(S^{31}\hat{u}_h^n + S^{32}\hat{v}_h^n + S^{33}\hat{w}_h^n\right) - \Delta tB^3\hat{p}_h^n = (rhs^n)_3 \\ (B^1)^T\hat{u}_h^n + (B^2)^T\hat{v}_h^n + (B^3)^T\hat{w}_h^n = 0 \end{cases} \quad (3)$$

where $M_{\varrho l}$ stands for the lumped mass matrix, S^{ij} corresponds to the given component of the viscous stress tensor matrix, and the pair $B^i/(B^i)^T$ represents the discrete gradient and divergence operator, respectively. The right hand side term stemming from the time level t^n is as follows:

$$rhs^n := M_{\varrho l}\vec{v}_h^{n-1} + \Delta t(\Theta - 1)S_\eta\vec{v}_h^{n-1}. \quad (4)$$

As usual for FEM, the global matrices are to be assembled from the local elementwise contributions. It means the restriction of the finite element mesh during the elementwise assembly to single elements, where the set $\{\phi_i\}$ specifies the basis functions spanning the Q_2 finite element space and $\{\varphi_k\}$ spanning the (discontinuous) P_1 space, respectively.

Concerning the physical properties, the density ϱ is assumed to be constant, whereas the viscosity η is calculated at each cubature point according to the given shear dependent rheological model.

From this point on, an additional adjustment of the system to be solved is related to the presence of internal moving boundaries. Their treatment in this particular case will be performed on the basis of the so-called Fictitious Boundary Method (FBM) which is a simple filtering-related technique decomposing the computational domain into a fluid and a solid subdomain [10]. The fluid domain is then treated as if no FBM was applied, and the solid subdomain interacts with the fluid subdomain in terms of the imposed internal Dirichlet boundary conditions (i.e. the rotational velocity components of the 'immersed'

screws). According to the given method, the only difficulty is to perform a distance computation for all dof's at every timestep, so to recover the updated filter vector coding the solid and the fluid subdomain. In general, the method allows to encounter arbitrary (defined on the basis of surface triangulated descriptions) geometrical configurations of the elements, provided appropriate signed distance computation libraries are available. For the moment we restrict ourselves to the so-called Erdmenger screw-profiles [7], which has the advantage that their description consists of arcs, which allows for straightforward signed distance computations. Finally, the solution of system (3) with the constraints imposed by the FBM methodology is realized within a standard operator splitting approach in the context of a Discrete Projection Method (DPM) [13, 14]. Before going into details let us write the system to be solved in a more compact form:

$$\begin{cases} \frac{1}{\Delta t} A \vec{v}_h^n - B \hat{p}_h^n = \frac{1}{\Delta t} rhs^n \\ B^T \vec{v}_h^n = 0, \end{cases} \quad (5)$$

where A represents the nonlinear system matrix of the form:

$$A := M_{gl} + \Delta t \Theta S_\eta. \quad (6)$$

The main idea of the DPM approach is to decouple the velocity and the pressure computation and to use a special Pressure-Poisson method. The arising algorithm consists of a prediction (satisfying momentum balance) and of a correction (satisfying mass conservation) step, as follows:

- prediction step I: solution of the nonlinear Burgers equation within a defect correction loop using the pressure field from the previous time step

$$A \tilde{v}^n = rhs^n + \Delta t B p^{n-1}, \quad (7)$$

with \tilde{v}^n denoting the intermediate velocity field.

- prediction step II: enforcing incompressibility of \tilde{v}^n by solution of a corresponding discrete Pressure-Poisson-like equation

$$P_\rho q = \frac{1}{\Delta t} B^T \tilde{v}^n \quad \text{with} \quad P_\rho := [B^T M_{gl}^{-1} B] \quad (8)$$

for the pressure update q .

- correction step III:

$$p^n = p^{n-1} - q, \quad (9)$$

$$\vec{v}^n = \tilde{v}^n - \Delta t M_{gl}^{-1} B q. \quad (10)$$

According to the fully consistent realization of the above described algorithm one should apply an outermost iterative loop, so that the solution pair (\vec{v}^n, p^n) satisfies both conservation of mass and momentum. Unfortunately, for practical reasons (due to dramatic increase of computational time) such a realization does not always pay off, and therefore the simplified realization (only one outermost iteration/timestep) enforcing explicitly only mass conservation is being used, which under the assumption of small timesteps provides a sufficient compromise between accuracy and computational cost [13, 14].

3 Mesh Deformation (MD) technique

From the engineering point of view the use of CFD software packages in industrial environment for simulation purposes is (mainly if not only) justified if the given simulation software fulfills the requirements put on its productivity measure, which is directly related to the absolute and relative time required for preprocessing and the simulation itself under the guarantee of a reasonable computational accuracy while sustaining a wide geometrical variability (i.e. arbitrary screw shapes in case of CRTSE simulations). The fulfillment of such a criterion helps to perform very efficient case studies not only with respect to operation conditions but also with respect to geometrical investigations, so that the results can directly be transferred onto the production level. The key to satisfy such a requirement in the framework of a twin-screw simulation software is addressed in this work on the basis of an easy-to-implement Mesh Deformation Technique embedded in case of unsteady flow simulations into an Arbitrary Lagrangian-Eulerian (ALE) framework. Aside from the underlying high order FEM-FBM discretization supported with parallel multigrid-based linear solvers, the above mentioned mesh deformation components guarantee the required flexibility of the developed simulation tool without deteriorating the convergence and accuracy properties of the basic solver [2, 10].

Before going deeper with the description of the Mesh Deformation (MD) technique developed for the simulation of TSEs we would like to point out that up to our knowledge such a realization was not reported before and its ability is not constrained only for TSE simulations, but by means of further adjustments (such as its blockwise realization) it is completely general and computationally reasonably cheap. The first important attribute making our approach different from others described in the literature is that the realization is only algebraic and not PDE based. However, as it is also realized in typical PDE based MD techniques, the core of our technique is related to a construction of the so-called monitor function $\mathcal{M}(\mathbf{x})$, being responsible for addressing the required size distribution of the resulting mesh elements while sustaining their original and this way constant connectivity. The carefully constructed monitor function is then transformed into a weight distribution $w(\mathbf{x})$ within an iterative (repetitive) algebraic mesh smoothing procedure, also known as "Laplacian" smoothing with the difference that these procedures have been so far preferred only to correct or smooth the deformed mesh predicted by classical PDE based techniques, which corresponds to an isotropic setting of the weight distribution $w(\mathbf{x}) = 1.0$. According to our realization, the time-expensive PDE prediction step can be completely skipped and equivalently substituted with an anisotropic counterpart of the Laplacian mesh smoother operating by means of a corresponding weight distribution w_j as follows:

$$\mathbf{x}_i^{\text{new}} = (1 - \omega) \cdot \mathbf{x}_i^{\text{old}} + \omega \cdot \frac{\sum_{j=1, n}^{\text{if } \exists e_{ij}} w_j \mathbf{x}_j^{\text{old}}}{\sum_{j=1, n}^{\text{if } \exists e_{ij}} w_j} \quad \text{for } i = 1, n \quad (11)$$

where \mathbf{x}_i are the mesh vertice coordinates, e_{ij} are the edges connecting the element vertices, ω is the underrelaxation parameter (usually set to 0.25), and n is the total number of mesh nodes. The only drawback, stemming from a strictly mathematical point of view is that we cannot guarantee or prove (yet) the properties of the generated deformed mesh, but as experienced on the number of processed examples we observe the robustness of the

proposed numerical technique. The construction of the monitor function $\mathcal{M}(\mathbf{x})$ is in fact arbitrary, it may reflect or combine different aims expected from the deformation since it can react on field data such as the shear-rate $\|\dot{\gamma}\|$ distribution, temperature gradients or a signed distance function $d(\mathbf{x})$ representing the distance distribution to the closest solid interface. Our choice is based on the latter, since this may help to adapt the mesh especially in the gap regions appearing on different locations during the rotation of the screws in the barrel of extruders. Due to the underlying FBM methodology the construction of a corresponding signed distance function is required anyway, since it makes it possible to separate the fluid domain from its counterpart - the solid (screw) domain. Accordingly, we propose to construct distance fields being evaluated with respect to the individual screws and the barrel itself ($d_{\text{LeftScrew}}, d_{\text{RightScrew}}, d_{\text{Barrel}}$). These distance distributions are then used to be converted into a Monitor function $\mathcal{M}(\mathbf{x})$ addressed by only one single field. According to the most important guidelines for the construction of such a conversion mechanism *a)* the number of cells covering the screw domain should be minimal - even for the price of poor aspect ratios - since they do not actively contribute to the resolution of the fluid domain, and *b)* the smallest elements should be located in the screw/fluid interface regions enhancing a maximal resolution of the underlying interface region. Assuming that the constructed distance field is negative inside of the solid domain and positive in the fluid domain we propose a conversion mechanism ($d_i \Rightarrow w_i$) as indicated in Fig. 1, where $d_{i=[\text{LeftScrew}, \text{RightScrew}, \text{Barrel}]}$ serves as input in millimeter units and provides the corresponding weights w_i as output. These individual weights are then casted into a unique single field weight distribution w as follows:

```

IF (d_i < 0)  w_i := 2.25 * ABS(d_i)
IF (w_i < 3)  THEN
  w_i := 2 + (3 - w_i)
ELSE
  w_i := 2 - 0.2 * (w_i - 3)
ENDIF
w_i := MAX(w_i, 1)

```

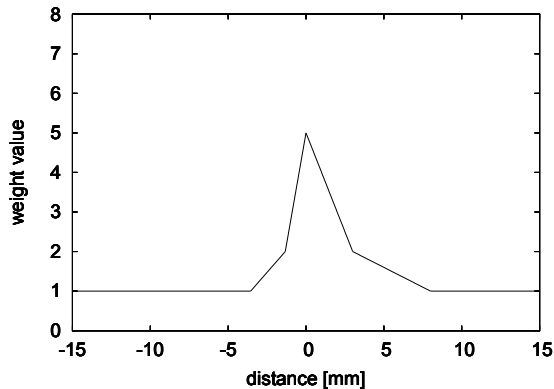


Figure 1: Left: construction of the weight distribution $w_i = f(d_i)$. Right: graphical representation of $w_i = f(d_i)$.

$$w = \text{MIN}(w_{\text{LeftScrew}} \cdot w_{\text{RightScrew}} \cdot w_{\text{Barrel}}, 25)^{2.5}$$

It is obvious from the formula above that the final weight distribution w is amplified exactly there where the two or even three input weight distributions have their maxima, i.e. the gap regions between the screws or between the screws and the barrel.

The only remaining step in the design of our weight distribution step is a normalization procedure that extends the usability of the method to general unstructured meshes as well, which is achieved by means of multiplying the previous weight distribution w with the element volume distribution function which one can obtain by means of an L_2 projection from the Q_0 (piecewise constant) space to the Q_1 (trilinear) space.

In order to gain a better insight into the mesh adaptation capability of the proposed MD method it is demonstrated in Fig.2 and Fig.3, which show the isotropically smoothed ($w = 1$) initial coarse mesh and its deformation after 3 successive refinements and three different cross-sections of the corresponding mesh used for a typical simulation of TSEs. It should also be pointed out that the generation of coarse meshes (according to the incorporated multigrid technique) for simulations is straightforward and can be fully automated by means of a block structured mesh generation function, as follows:

$$\text{Computational_Mesh} := f(n_r, n_\alpha, n_\beta, n_z, R_{\text{in}}, R_{\text{out}}, A, L, h)$$

where the parameters $n_r, n_\alpha, n_\beta, n_z$ are the number of required cells in the radial, outer circumferential, shared circumferential, and longitudinal direction and the geometrical parameters $R_{\text{in}}, R_{\text{out}}, A, L$ represent the inner/outer radius of the barrel, axis distance between the rotation axis, length of the barrel and the parameter h represents the height of the cut flattening the connection regions of the barrels. Aside from the advantage of reducing the preprocessing time spent on mesh generation (definition of boundary conditions) to a negligible amount such a function based mesh generation plays a key role in performing mesh convergence studies and CRTSE performance case studies, as well.



Figure 2: Block structured coarse mesh (Level 1) (left) postprocessed by means of the proposed MD technique with respect to the implicitly given screw geometry (middle) leading to the fine level (Level 3) computational mesh (right).

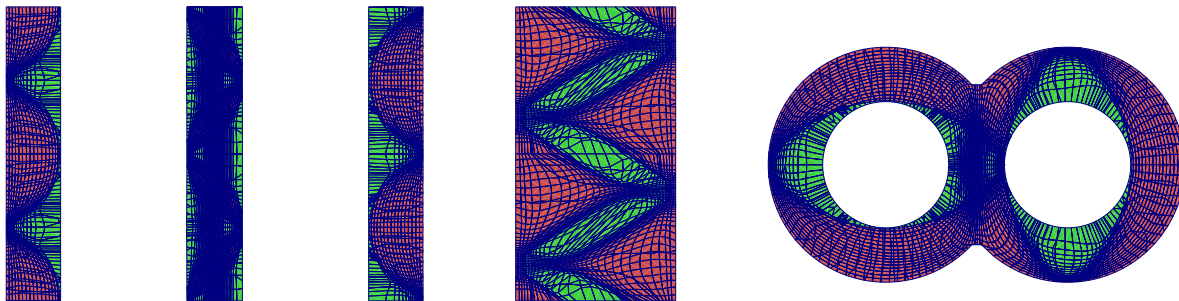


Figure 3: Result of the proposed MD technique. Views of different cutplanes perpendicular to the cartesian axis. Regions colored with orange/green represent the fluid/solid domains.

Concerning the ALE framework we follow its computationally cheapest, simplest but best understood Backward Euler realization [18] which under the assumption of small timesteps is still a reasonable candidate especially in light of the highly non-linear shear dependent rheological fluid properties, which already pose certain restrictions on the timestep size due to stability reasons. The mesh velocity is also evaluated in a simple way, as the change of location of the mesh nodes divided by the timestep size, however, it is very important to remark that the input mesh into the corresponding MD step at the given timestep is identical to the already deformed mesh used in the previous timestep. This way, one can achieve a more or less continuous motion of the mesh, which is a prerequisite to a proper realization of the ALE framework [18]. According to our realization the regulation of the mesh velocity is achieved by the number of anisotropic Laplacian smoothing steps which is on the order of 64 during the initialization but only on the order of 4-8 during the unsteady simulations depending on the timestep size.

4 Summary of practical simplifications

Having in mind the computational efforts required for accurate simulations of non-Newtonian flows in TSEs especially in a framework of extensive parameter studies one should exploit as much of justified simplifications as possible so to optimize the overall computational costs. From this point of view there are three recommended simplifications which under certain circumstances may dramatically accelerate the individual computations. These are the following ones:

- periodic boundary conditions
- moving reference frame
- 'false' time-stepping

In the following we will discuss the advantages which these simplifications offer and the conditions under which their usage is justified.

The use of periodic boundary conditions possesses a great potential especially in case studies involving different mixing elements because it may provide valuable information on the characteristics of given segments under the assumption that the segment repeats itself at least several times in the surrounding of the analyzed extrusion segment. An other benefit of this simplification lies in the reduction of the computational domain, which otherwise should contain an artificial inflow/outflow region being responsible only for providing a relaxation region before entering and after leaving the mixing region contributing with an unwanted computational overhead. The only disadvantage that this simplification suffers of is the fact that flowrates can be only indirectly imposed by means of variation of the corresponding pressure drop values implicitly addressing the requested volumetric throughput. The use of a moving reference frame in the context of TSEs is restricted only to computational analysis of infinitely long smooth (without secondary structures) conveying elements since it can be exploited that if the computational frame moves exactly with the velocity $v_{\text{Frame}} = L_{\text{Pitch}} f_{\text{Rot}}$ (L_{Pitch} stands for the pitch length and f_{Rot} for the rotation speed of the mixers) the mixers resemble a steady geometry possessing the rotational (inner) Dirichlet boundary conditions and the reference frame velocity at the same time. Due to relying on the infinitely long TSE assumption it is

straightforward to combine this simplification with periodic boundary conditions gaining a special insight into the problem in question being described with only one "pseudo steady" solution representing the full nonstationary process.

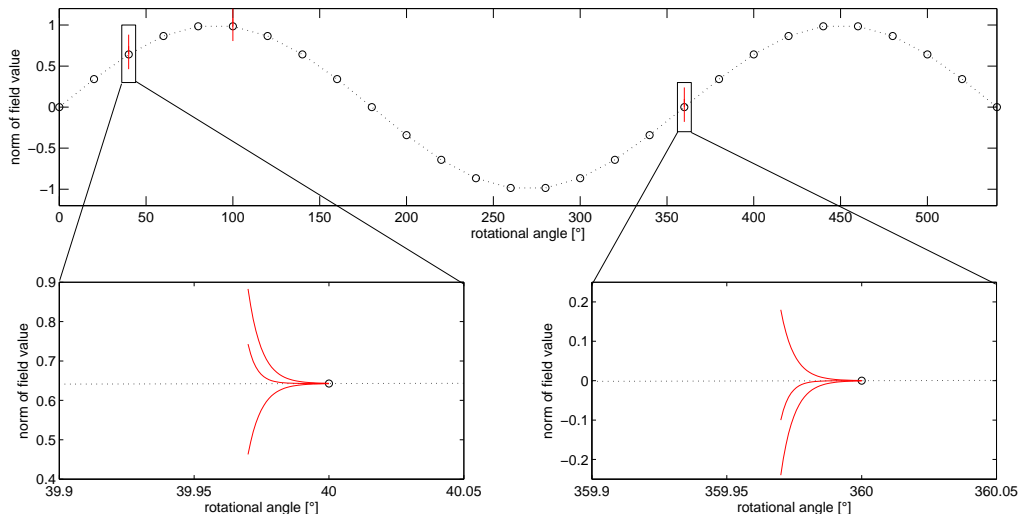


Figure 4: Schematical realization of the 'false' time-stepping method covering the full 2π rotation space with 20° spacing.

Another challenge of the numerical simulation of CRTSEs is arising due to the various physical time scales present in the underlying flow problem. In order to give a deeper physical insight it is worthwhile to mention the time scales of the momentum diffusion $\tau_d \approx 10^{-5} - 10^{-4}s$ (assuming representative molecular viscosities are on the order of $< 10^5 Pa \cdot s$) and the time scale of the process itself $\tau_r \approx 10^0s$ (assuming rotational frequencies $\approx 60 min^{-1}$) according to which the viscous forces are clearly dominating the inertial forces (Stokes flow). As a result the flow is somewhat without a memory or in other words: it is expected that any kind of perturbations such as changing inflow conditions or flow structures past internal obstacles or screws neither arise nor sustain for a long time ($t - t_0 \gg \tau_d$). From a practical point of view this means that even in case of a transient simulation corresponding to the same geometrical configuration of the screws a pseudo-steady state is reached already after a simulation time on the order of $\approx 10^{-5} s$ regardless of the imposed initial conditions (i.e. velocity and pressure distributions over the fluid domain). Consequently, this enables the extension of the transient simulation of the process into a 'false' time-stepping framework whereas a series of (independent) transient (or even steady [3, 8]) simulations are to be performed covering the available range of screw superposition angles (which can be often less than 360° depending on the particular screw geometry). A schematical realization of the technique is demonstrated in Fig. 4, which addresses the time evolution of a pseudo quantify (referring to overall pressure drop, specific power consumption, distribution of shear rates or even local velocity, pressure, etc.) in time computed for a series of 20° superposition angles and for different initial conditions (subpictures). This simplification offers itself to be useful for screw geometries being different than the classical conveying screws (i.e. conveying screws with secondary structures - SME [11] - or kneading elements). In these cases we follow a strategy to cover

the range of screw superposition angles by 3° spacing so to get a comprehensive picture into the full transient flow dictated by the geometrical changes.

5 Convergence Analysis of the Developed Numerical Scheme in Applications to CRTSEs

This section is devoted to a mesh convergence study with respect to a typical performance analysis of CRTSEs. Such performance analysis are well established procedures from the available literature [16, 17] and are carried out in order to characterize or to compare the operation of one mixing screw element against another. Concerning the reconstruction of the screws we follow the strategy proposed by Booy [4] (see Fig. 5) which has been due to its excellent geometrical properties (the clearance between the screws is during the whole rotation constant) successfully established in practice (i.e. [1]). The required set of parameters uniquely defining the geometrical description of the computationally analyzed screw and barrel is addressed in Tab. 1, where all the parameters have been defined in the previous section except for the two clearances $\Delta_{S/B}$ and $\Delta_{S/S}$ defining the Screw/Barrel and the Screw/Screw gap sizes (in fact, $\Delta_{S/S}$ is redundant since its value is identical to $A - R_{\text{Out}} - R_{\text{In}}$).

Table 1: Complete set of the used geometric parameters.

$R_{\text{Out}} = 20 \text{ mm}$	$R_{\text{In}} = 10 \text{ mm}$	$A = 30.4 \text{ mm}$	$L = 30 \text{ mm}$
$h = 1 \text{ mm}$	$\Delta_{S/B} = 0.4 \text{ mm}$	$\Delta_{S/S} = 0.4 \text{ mm}$	$L_{\text{Pitch}} = 60 \text{ mm}$

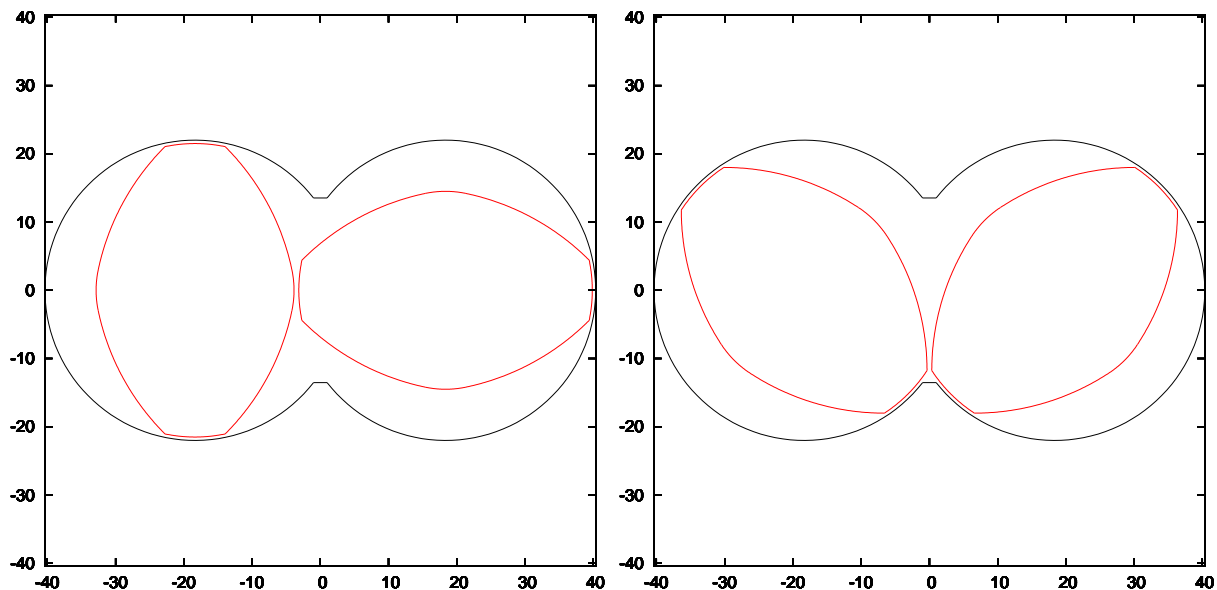


Figure 5: Geometrical construction of the screws according to Booy [4].

According to industrial experience related to synthetic rubber processing we have chosen a model material experiencing shear thinning rheological properties described by

the Ellis model of the following form

$$\mu = \mu_0 \cdot \frac{1}{1 + \left(\frac{\|\dot{\gamma}\|}{\|\dot{\gamma}_0\|} \right)^\alpha} \quad (12)$$

closed by the values of parameters given in Tab. 2 covering the behavior of typical synthetic rubbers often processed in industrial scales.

Table 2: Parameters defining the Ellis rheological model.

$\mu_0 = 10^5 \text{ Pa} \cdot \text{s}$	$\ \dot{\gamma}_0\ = 10^{-0.1} \cdot \text{s}^{-1}$	$\alpha = 0.8$
--	--	----------------

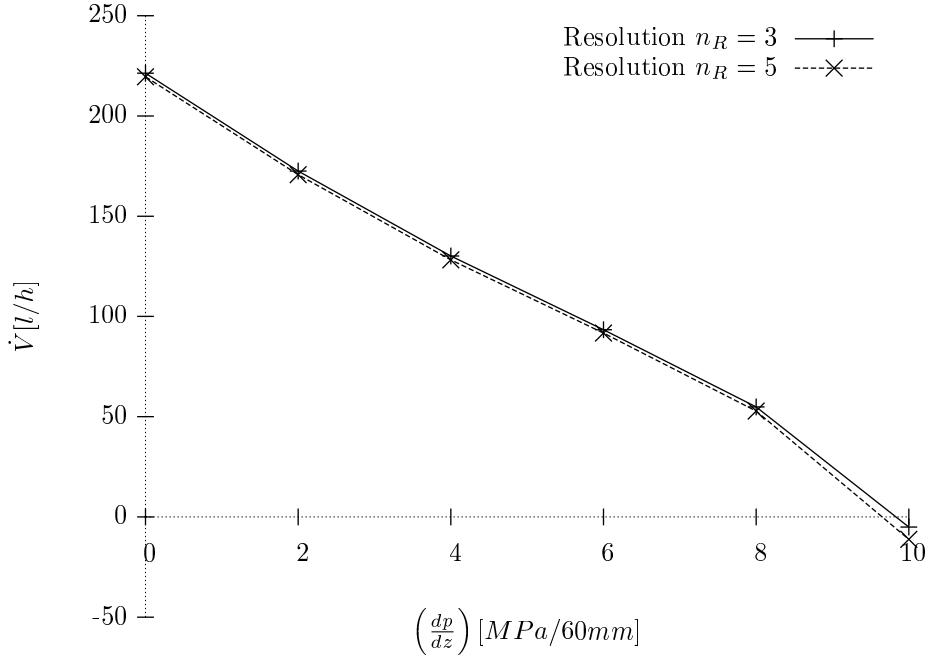


Figure 6: Flowrate characteristics of the computationally analyzed screw segment for different pressure drops evaluated for two mesh resolutions.

The only remaining parameters required for a unique definition of our test case are related to the operation conditions out of which only the rotational frequency is free (set to $f_{\text{Rot}} = 120 \text{ min}^{-1}$) while the pairs of volumetric flow rates - \dot{V} - and pressure drops - $(\frac{dp}{dz})$ - are to be determined to cover the industrially interesting region of operation conditions constrained by $\left[(\frac{dp}{dz}) = 0, \dot{V} = \max \right]$ and $\left[(\frac{dp}{dz}) = \max, \dot{V} = 0 \right]$. In the following, we demonstrate the computationally obtained results for such a parameter study in the framework of a mesh convergence study so to reveal the accuracy of the developed simulation tool. For this purpose there were generated two block structured hexahedral coarse meshes (Level 1) which have been 3 times successively refined (2x2x2) and deformed according to our proposed MD mechanisms described in the previous section. The parameters of the two coarse meshes were the following:

- Mesh 1: $n_r = 3, n_\alpha = 14, n_\beta = 6, n_z = 8$ resulting in $1,008 \times 8 \times 8 = 64,512$ elements

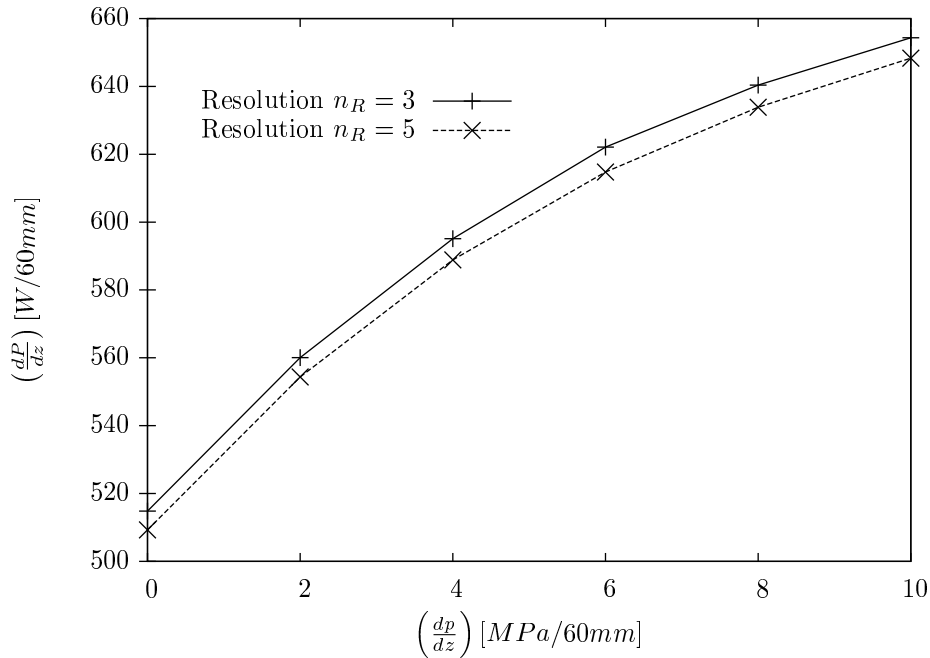


Figure 7: Power consumption characteristics of the computationally analyzed screw segment for different pressure drops evaluated for two mesh resolutions.

- Mesh 2: $n_r = 5, n_\alpha = 22, n_\beta = 10, n_z = 12$ resulting in $3,960 \times 8 \times 8 = 253,440$ elements

As an additional remark concerning the generated meshes, it is worth to be mentioned that the meshes have been extruded to only a half a pitch length in the axial direction due to the underlying periodicity which is this way fully exploited. Since in this section we aim mainly to demonstrate the major advantages of the proposed numerical techniques (high order FBM-FEM with MD) in the framework of a convergence study we employed the simplifications of periodic BCs and moving reference frame (introduced in the previous section) so to contribute with a benchmark configuration to the CFD community specialized to CRTSEs. The mesh convergence of the proposed numerical scheme on the introduced CRTSE benchmark is demonstrated in terms of integral extrusion characteristics $\dot{V} = f\left(\frac{dp}{dz}\right)$ and $\frac{dP}{dz} = f\left(\frac{dp}{dz}\right)$ in the corresponding Fig. 6 and 7 such as in terms of volumetric shear rate distributions (Fig. 8) and cross-sectional field distributions (Fig. 9). As it can be seen from the mentioned figures a satisfactory convergence – fulfilling less than 5% tolerances required by engineers – is achieved.

6 Numerical Simulation of CRTSEs - full case study

In this section we will give an insight into a typical case study of CRTSEs demonstrating the capabilities of our developed computational method. Since one of the main benefits of our proposed methodology is related to its favorable productivity measure (i.e. negligible preprocessing time for nearly arbitrary geometrical complexity guaranteeing a reasonable computational accuracy), it is more than natural to investigate its performance in a typical case study, which is intended to provide the necessary information to a process engineer

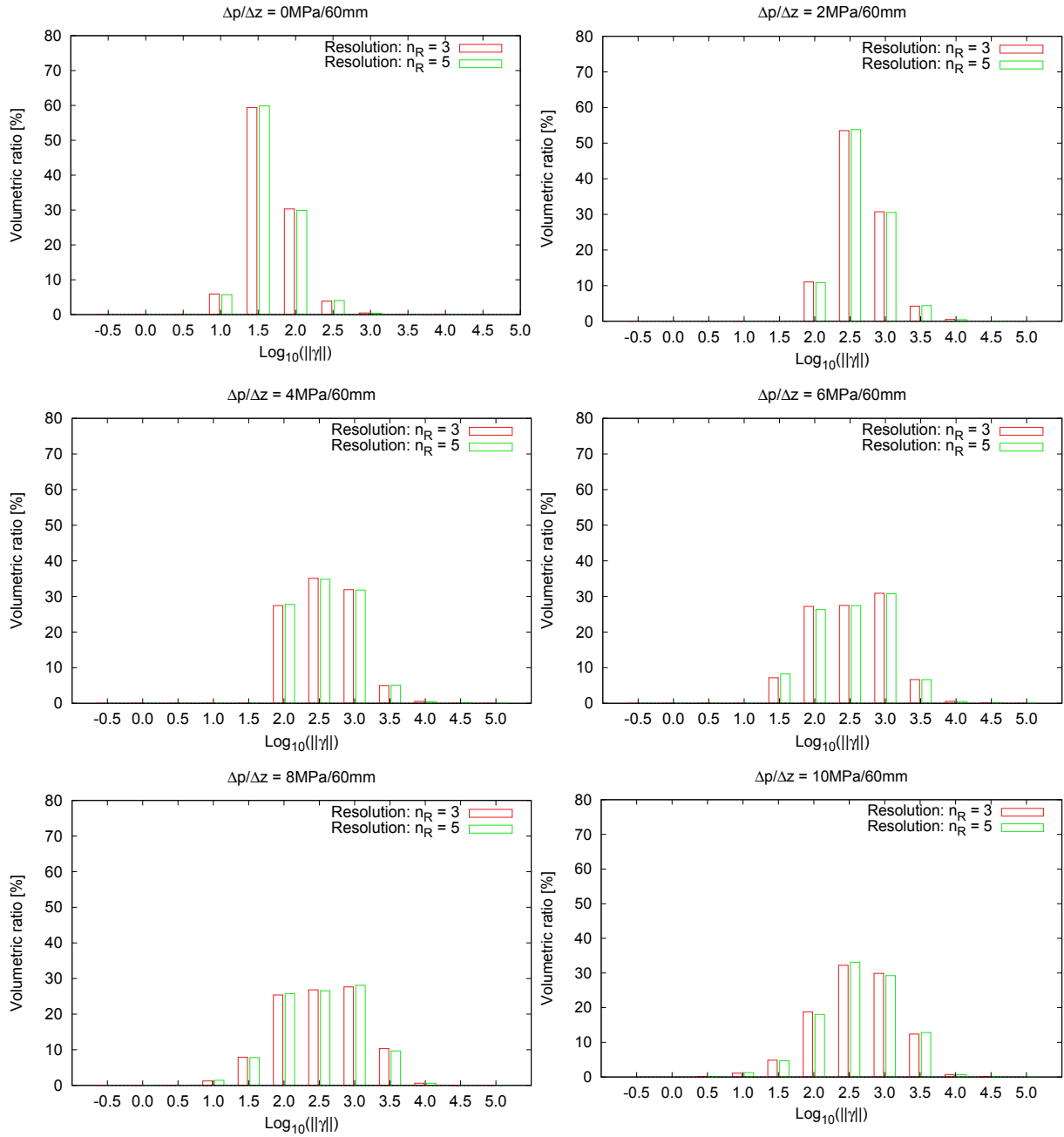


Figure 8: Mesh convergence of shear stress distribution in histogram representation for different pressure drops.

during the design of a particular TSE machine for a process under consideration. For this purpose six very similar cases will be analyzed, with the only difference of given geometrical details and their respective influence onto the main process parameters. Operational conditions, fluid parameters and the main geometrical parameters (Pitch length L_{Pitch} , axial distance A and inner/outer barrel radii R_{Out} , R_{In}) are considered to be the same and equal to the values introduced in the previous section. The first three cases (Case 1a, 1b, 1c) are corresponding to the previously introduced continuous two-flighted elements, but with varying Screw/Barrel and Screw/Screw gap sizes ($\Delta_{S/B}, \Delta_{S/S}$ - see Tab.3).

The second set of cases (Case 2a, 2b, 2c) corresponds to screw segments characterized

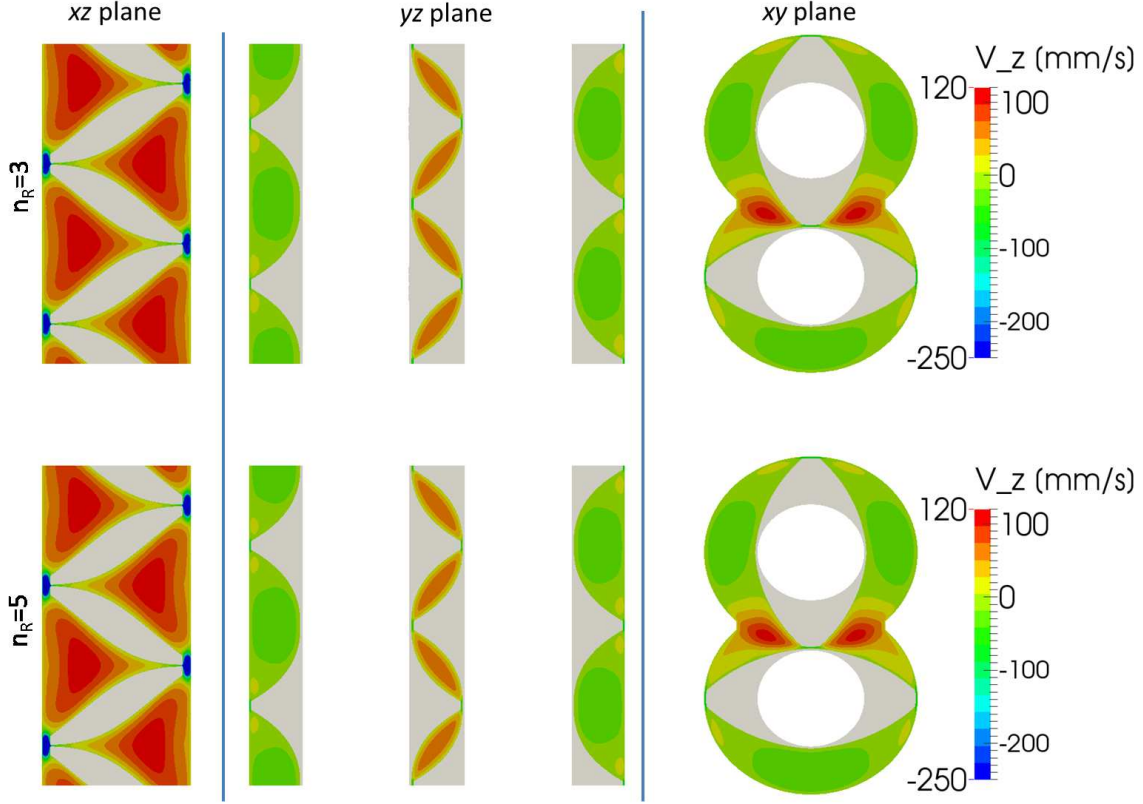


Figure 9: Convergence of the axial velocity distribution in three different orthogonal cutplanes.

Table 3: Considered gap size parameters for Cases 1a, 1b, 1c.

Case 1a	Case 1b	Case 1c
$\Delta_{S/B} = \Delta_{S/S} = 0.4 \text{ mm}$	$\Delta_{S/B} = \Delta_{S/S} = 0.2 \text{ mm}$	$\Delta_{S/B} = \Delta_{S/S} = 0.5 \text{ mm}$

with secondary structures. The construction of such screw elements is achieved by the intersection of the continuous screw elements with a circular cut-off function periodically rotated within a certain cut-off pitch length for a certain number of evenly distributed (same offset angle) cut-off circles. The rotation radius of the cut-off circles coincides with the outer radius of the screws ($R_{\text{Out}} - \Delta_{S/B}$) and they are rotated around the identical axis as the screws' rotation axis. The two-dimensional construction of the screws is addressed in Fig. 10 and the three-dimensional realization of the underlying cases is displayed in Fig. 11. In order to have a comparison on the same basis we considered for the Cases 2a, 2b, 2c the same radii of the cut-off circles $R_{\text{CutOff}} = 5 \text{ mm}$ and also the same resulting number of secondary structures per screw pitch length ($\frac{N_{\text{CutOff}}}{L} = 6$), which is achieved by adjusting the number of cut-off circles $N_{\text{CutOffCircle}}$ (or cut-off offset angle) and the cut-off pitch length (L_{CutOff}). The complete set of parameters uniquely defining the shape of the considered screws is shown in Tab. 4.

Concerning the simplifications used for the simulations, for Cases 1a,1b, 1c we used the periodic boundary conditions with the reference frame velocity transformation, while

Table 4: Considered gap size parameters for Cases 2a, 2b, 2c.

parameter	Case 2a	Case 2b	Case 3c
L_{CutOff}	∞	60 mm	15 mm
$N_{\text{CutOffCircle}}$	6	4	2
$\Delta_{S/B}, \Delta_{S/S}$	0.4 mm	0.4 mm	0.4 mm

for Cases 2a, 2b and 2c we used the periodic boundary conditions with the 'false' time-stepping technique, since the solution becomes periodically (in time) transient due to the different superposition of the secondary structures on the screws. According to the underlying 'false' time-stepping technique, a sequence of simulations for 3° offset angles has been performed and averaged for postprocessing reasons. The obtained flowrate and power consumption characteristics on basis of the time averaged mean values and deviations have been compared with the other three cases (1a, 1b, 1c) in Fig. 12 and Fig. 13. As it can be seen from the comparisons the responses on the introduced deviations are clearly distinguishable, moreover, in hand of a process engineer they may play a significant role in the design of the extruder to achieve the goals expected from the overall extrusion process. It is obvious that more detailed representations of the resulting field data would further contribute to the understanding of the process, such as histograms of shear rate distributions (as shown in the previous section), estimation of the integral or even local heat release (due to internal friction) intensity.

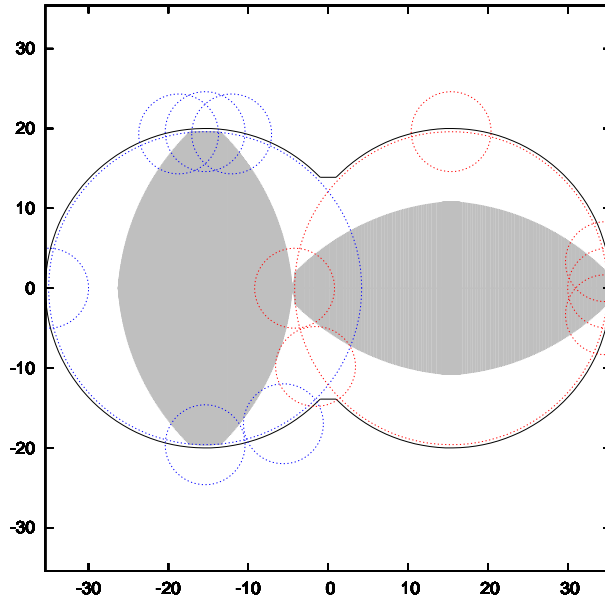


Figure 10: Geometrical construction of the screws with secondary structures.

7 Conclusions

In this paper we have presented a novel computational strategy, which exploits the features of its individual components and offers the advantage to be casted to a black-box simulation tool conditioned only with minimum preprocessing requirements. As shown

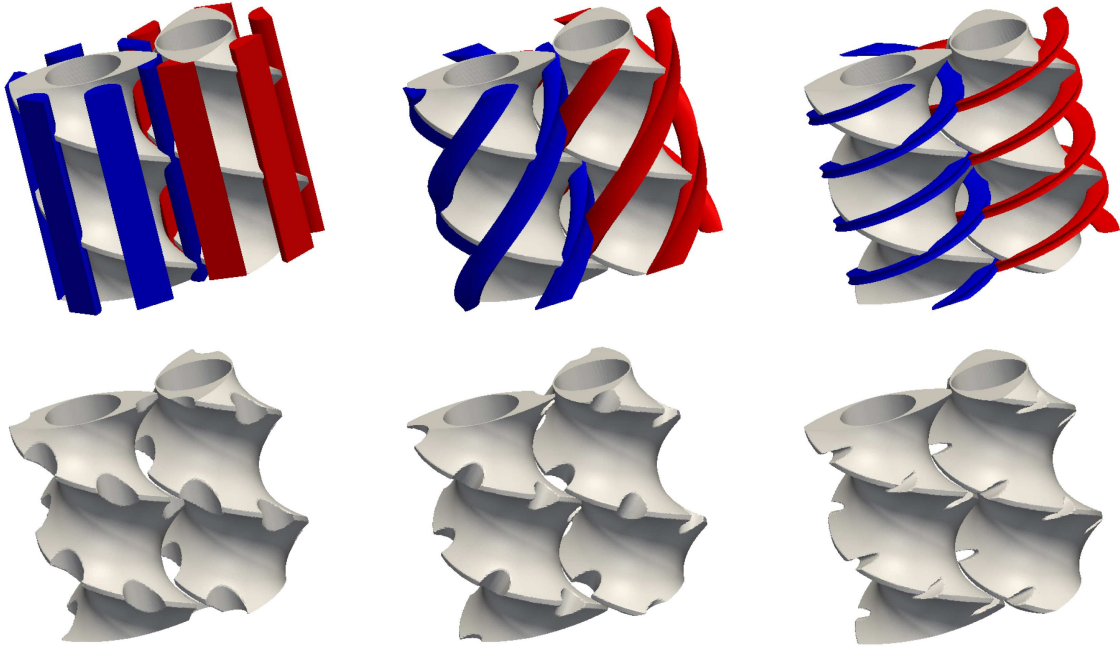


Figure 11: Geometrical construction of the considered secondary screw profiles for Case 2a, Case 2b and Case 2c.

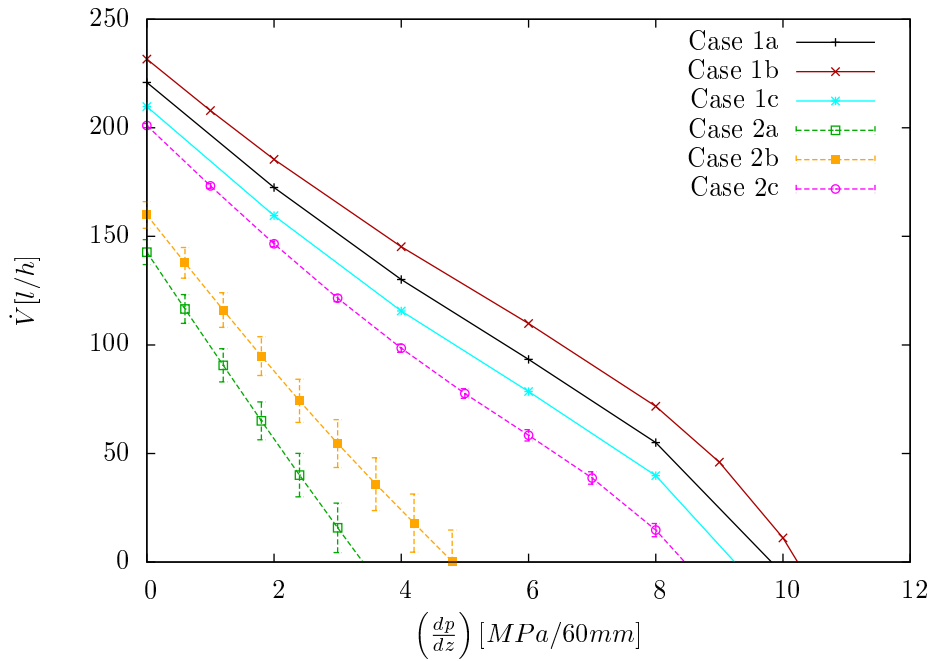


Figure 12: Flowrate characteristics for the computationally analyzed screw segments.

in the numerical example in the framework of a mesh convergence study the prototype of such an engineering tool guarantees a reasonably high accuracy and is flexible to predict the responses of the material processing operations aside of changes of operation con-

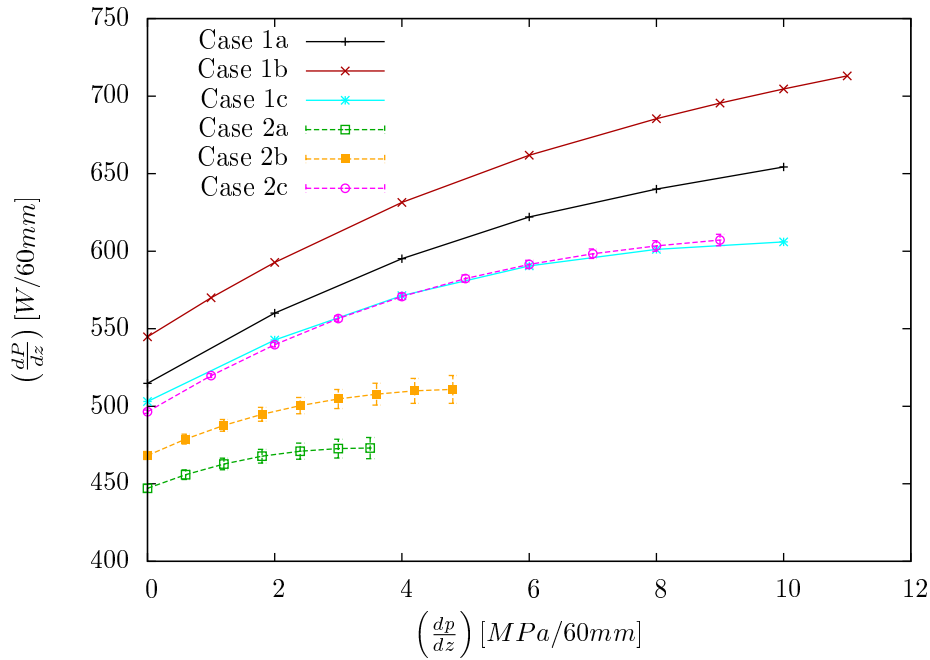


Figure 13: Power consumption characteristics for the computationally analyzed screw segments.

ditions, physical parameters and geometrical changes involving secondary structures, as well. The extension of the capabilities of such a simulation tool to single-, triple- or even arbitrary number screw extruders, such as the extension of the screw descriptions from implicit (in terms of functions) to fully general surface triangulations (i.e. STL description) is straightforward.

Acknowledgments

Financial support of DFG (SFB 708 TP-B7, TU 102/43-1), AiF and the SIGMA common research project is gratefully acknowledged. Calculations have been carried out on the LiDong cluster at TU Dortmund. We would like to thank the LiDong cluster team for their help and support.

References

- [1] Alsteens B., Legat V. and Avalosse Th., *Parametric study of the mixing efficiency in a kneading block section of a twin-screw extruder*, University of Louvain, 2004.
- [2] Bayraktar E., Mierka O., Turek S., *Benchmark Computations of 3D Laminar Flow Around a Cylinder with CFX, OpenFOAM and FeatFlow*, International Journal of Computational Science and Engineering, **7**-(3), pp:253–266, 2012, doi: 10.1504/IJCSE.2012.048245

- [3] Bertrand F., Thibault F., Delamare L. and Tanguy P.A., *Adaptive finite element simulations of fluid flow in twin-screw extruders*, Computers & Chemical Engineering, **27**-(4), pp:491–500, 2003, ISSN 0098-1354, doi: 10.1016/S0098-1354(02)00236-3.
- [4] Booy, M.L., *Geometry of Fully Wiped Twin-Screw Equipment*, Polymer Engineering & Science, **18**, pp:973984, 1978, doi: 10.1002/pen.760181212
- [5] Damanik, H., Hron, J., Ouazzi, A., Turek, S., *A monolithic FEM approach for the log-conformation reformulation (LCR) of viscoelastic flow problems*, J. Non-Newtonian Fluid Mech., **165**(19-20), pp: 1105–1113, 2010, doi:10.1016/j.jnnfm2010.05.008.
- [6] Damanik, H., Hron, J., Ouazzi, A., Turek, S., *Monolithic Newton–multigrid solution techniques for incompressible nonlinear flow models*, International Journal for Numerical Methods in Fluids, **71**, pp: 208–222, 2012, doi: 10.1002/fld.3656.
- [7] Erdmenger R., *Mehrwellen Schnecken in der Verfahrenstechnik*, Chem. Ing. Tech., **36**, pp:175–185, 1964.
- [8] Héту J.-F., Ilinca F., *Immersed boundary finite elements for 3D flow simulations in twin-screw extruders*, Computers & Fluids, **87**-(25), pp:2–11, 2013, doi: 10.1016/j.compfluid.2012.06.025
- [9] Kohlgrüber K., *Der gleichläufige Doppelschneckenextruder Grundlagen, Technologien, Anwendungen*, Carl Hanser Verlag, München, 2007.
- [10] Münster R., Mierka O. and Turek S., *Finite element-fictitious boundary methods (FEM-FBM) for 3D particulate flow*, International Journal for Numerical Methods in Fluids, **69**, pp:294–313, 2012, doi: 10.1002/fld.2558
- [11] Sarhangi Fard, A. and Anderson, P. D., *Simulation of distributive mixing inside mixing elements of co-rotating twin-screw extruders*, Computers & Fluids, **87**, pp:79–91, 2013, doi: 10.1016/j.compfluid.2013.01.030
- [12] Sarhangi Fard, A., Hulsen, M. A., Meijer, H. E. H., Famili, N. M. H. and Anderson, P. D., *Adaptive non-conformal mesh refinement and extended finite element method for viscous flow inside complex moving geometries*, International Journal for Numerical Methods in Fluids, **68**, pp:1031–1052, 2012, doi: 10.1002/fld.2595
- [13] Turek S., *On discrete projection methods for the incompressible Navier-Stokes equations: an algorithmical approach*, Computer Methods in Applied Mechanics and Engineering, **143**(3-4), pp:271–288, 1997, doi: 10.1016/S0045-7825(96)01155-3.
- [14] Turek S., *Efficient Solvers for Incompressible Flow Problems, An Algorithmic and Computational Approach*, Lecture Notes in Computational Science and Engineering, **6**, Springer-Verlag, 1999.
- [15] White J.L., *Twin-Screw Extrusion, Technology and Principles*, Carl Hanser Verlag, New York, 1991.
- [16] Zhu X.Z., Xie Y.J. and Yuan H.Q., *Numerical Simulation of Extrusion Characteristics for Co-rotating Tri-Screw Extruder*, Polymer-Plastics Technology and Engineering, **46**-(4), 2007, pp:401–407, doi: 10.1080/03602550701242919.

- [17] Zhu X.Z., Xie Y.J. and Yuan H.Q., *Numerical Simulation of Flow Characteristics of Co-Rotating Intermeshing Four-Screw Extruders*, Journal of Reinforced Plastics and Composites, **27**, 2008, pp:321–334, doi: 10.1177/0731684407084115.
- [18] Donea von J., Huerta A., *Finite Element Methods for Flow Problems*, John Wiley & Sons, 2003, ISBN-10: 0471496669.